# CHAPTER 6

# STUDIES ON SUBSTITUTED PEROVSKITE CATALYSTS

## 6.1 Introduction

Many types of catalysts for the DPF have been investigated for the soot combustion; platinum group metals (PGM), Perovskite-type oxides, spinel type oxides and mixed transient metal oxides [Mishra and Prasad 2014]. Most of the perovskite-type oxides ($ABO_3$), meet the requirements for soot oxidation, and thus many kinds of bulk perovskite-type oxides have been prepared and studied in order to improve the performances for soot oxidation. The redox property of a perovskite-type oxide is closely related to the nature of B-site or A-site cations, some researchers [Teraoka et al. 1995, Teraoka et al. 1996, Burch and Coleman 1999] have proved that the perovskite-type oxide catalysts exhibit much better catalytic performances for the title reaction than that of simple oxide. Perovskite structure tolerates partial substitution of both A- and B-sites cations with other elements, leading to the generation of oxygen vacancies or the change of valence of A- and/or B-site cations; as a result, the activity is often improved. When the A-site cations are partially substituted by the cations with lower valance, such as alkali metal ions, the oxidation state of B-site cations will be increased or some oxygen vacancies are generated in order to maintain the electrical neutrality.

The formed higher valence ions usually possess higher catalytic activity for soot oxidation [Li et al. 2010, Li et al. 2012], and the formed oxygen vacancies are favourable to oxygen transferring. It is generally thought that the adsorbed oxygen species such as $O^{2-}$ and $O^{-}$ often locate at oxygen vacancies on perovskites surface [Yamazoe and Teraoka 1990], which are main active oxygen species for soot combustion [Liu et al. 2008, Fino et al. 2003]. Their nature largely depends on the character of B-site ions and the substituted amount of A-site ions by lower valance ions [Yamazoe and Teraoka 1990]. When the A-site ions in perovskites are partially substituted by lower valance ions such as potassium or strontium ions, the catalytic activity towards soot combustion is often improved [Peng et al. 2007, Teraoka et al. 2001].

In this chapter, the physico-chemical properties and catalytic performances of Ni-, Co-, Fe- and Zn- based perovskite-type complex oxide catalysts and substitution of A-site by Sr and B-site by M (M = Cu, Fe and Ni) of $LaCoO_3$ were comparatively and systematically studied to clarify the effect of substitutions of cations. The perovskite structure tolerates partial substitution of both A- and B-sites cations with other elements. The effects of the intrinsic factors including nature of B-site ions, redox properties of perovskite-type composite oxide catalysts, and the external factors containing contact model of catalyst and soot, and the gas hourly space velocity (GHSV) on their catalytic performances for the elimination of soot particles from diesel exhaust were also investigated.

## 6.2 Experimental

### 6.2.1 Synthesis of Perovskite Type Catalysts

A series of perovskite-type oxide catalysts were prepared by the citric acid sol-gel method. All AR-grade chemicals were used in the preparation of catalysts. Three

different set of La based perovskite, $LaCoO_3$, $LaFeO_3$ and $LaNiO_3$, were prepared by the sol-gel method. For the preparation of $LaCoO_3$ aqueous solution (0.1M) of $La(NO_3)_3.6H_2O$ and $Co(NO_3)_2.6H_2O$ were mixed with citric acid that was equivalent in gram mole with that of the total cations ($La^{3+}$ and $Co^{2+}$). Resulting red wine colored solution was heated at 80$^oC$ under continuous stirring. After 3h of continuous stirring the clear solution gradually transformed into gel which was translucent and viscous. The wet gel was dried homogeneously overnight in an electric oven at 120$^oC$. The obtained loose and foamy pink color solid was heated in two steps. First heating at 600$^oC$ for 1h is carried out to decompose the organic and second step of calcination was done at 750$^oC$ for 4h to obtain hazy black porous solid. $LaFeO_3$ and $LaNiO_3$ perovskite were prepared in the similar fashion from their nitrate precursors $Fe(NO_3)_3.9H_2O$ and $Ni(NO_3)_2.6H_2O$ respectively.

A mixed metal oxide $LaZnO_y$ with same stoichiometric composition as required for perovskite formation $LaZnO_3$ was also prepared by the citric acid sol-gel method. Aqueous solution (0.1M) of $La(NO_3)_3.6H_2O$ and $Zn(NO_3)_2.6H_2O$ were mixed with citric acid that was equivalent in gram mole with that of the total cations ($La^{3+}$ and $Zn^{2+}$). Resulting colourless solution was heated at 80$^oC$ under continuous stirring. After 3h of continuous stirring the clear solution gradually transformed into gel which was translucent and viscous. The wet gel was dried homogeneously overnight in oven at 120$^oC$ in presence of air. Obtained off-white colored loose and foamy solid was heated at 600$^oC$ for 1h and further grained before calcining it at 750$^oC$ for 4h and finally obtained white colored porous solid.

In the second step series of single substituted perovskite $La_{1-x}Sr_xCoO_3$ were prepared. For the preparation of $La_{1-x}Sr_xCoO_3$ (x=0.1-0.4) aqueous solution (0.1M) of each $La(NO_3)_3.6H_2O$, $Co(NO_3)_2.6H_2O$ and $Sr(NO_3)_2$were mixed with citric acid which

was equivalent in gram mole with that of the total cations ($La^{3+}$, $Sr^{2+}$ and $Co^{2+}$). Resulting red wine colored solution was heated at 80$^{o}$C under continuous stirring. After 3h of continuous stirring the clear solution gradually transformed into a gel which was translucent and viscous. The wet gel was dried overnight in an electric oven at 120$^{o}$C in stagnant air. Obtained loose and foamy pink color solid was calcined in two steps. First, heating at 600$^{o}$C for 1h was carried out to decompose the organic matters and second step of calcination was done at 750$^{o}$C for 4h, to obtain a black porous solid.

In the next step series of double substituted perovskite $La_{0.9}Sr_{0.1}Co_{0.5}M_{0.5}O_3$ (M= Fe, Ni and Cu) were prepared by the sol gel method using nitrate precursors of the constituent elements in appropriate ratio as followed above. Here also the dried solid precursor was calcined in two steps as mentioned in the case of the first type of the catalyst preparation.

$La_{0.95}Pd_{0.05}Co_{0.5}Fe_{0.5}O_3$ Perovskite catalyst was prepared by sol gel method using chloride precursor of palladium and nitrates of other constituents elements in appropriate ratio by following the same steps of preparation for other catalysts.

### 6.2.2 Catalytic Activity Measurements

The catalytic performances of the prepared catalysts for oxidation of soot were evaluated in a compact fixed bed tubular quartz reactor as shown in figure 3.9 and discussed in section 3.6.2. To verify the reproducibility of the experimental data each experiment was performed twice repeatedly for the soot oxidation.

### 6.2.3 Catalyst Characterization

The textural characterisation of the catalysts was carried out by low temperature $N_2$-sorption method using a Micromeritics ASAP 2020 analyzer. Phase identification of the catalysts were carried out by X-ray diffraction (XRD) patterns on a powder X-ray diffractometer (Rigaku Ultima IV) using CuKα1 (λ = 1.5405 Å) radiation with a nickel

filter operating at 40mA and 40kV. FTIR spectra of the catalysts were recorded in the range of 400-4000 $cm^{-1}$ on Shimadzu 8400 FTIR spectrometer with KBr pellets at room temperature. XPS of the catalysts was performed on an Amicus spectrometer equipped with Mg Kα X-ray radiation. For typical analysis, the source was operated at a voltage of 15 kV and current of 12 mA. Pressure in the analysis chamber was less than $10^{-5}$ Pa. The binding energy scale was calibrated by setting the main C 1s line of adventitious impurities at 284.7 eV, giving an uncertainty in peak positions of ±0.2 eV. The surface morphology was studied with FEI Quanta 200 scanning electron microscope (SEM) instrument. An accelerating voltage of 30kV and magnification of 1000 and 20000x were applied.

## 6.3 Results and Discussion

### 6.3.1 Textural Characterization of the Catalysts

Typical nitrogen physisorption isotherms and pore size distribution curves for the substituted perovskite catalyst $La_{0.9}Sr_{0.1}CoO_3$, $La_{0.9}Sr_{0.1}Co_{0.5}Ni_{0.5}O_{3-\delta}$, $La_{0.9}Sr_{0.1}Co_{0.5}Cu_{0.5}O_{3-\delta}$ and $La_{0.9}Sr_{0.1}Co_{0.5}Fe_{0.5}O_{3-\delta}$ prepared by sol gel method and calcined at 750$^oC$ are shown in Figures 6.1 and 6.2 respectively. The nitrogen sorption isotherms exhibit type-IV isotherms with H1 type hysteresis loop. This type of isotherm occurs on porous adsorbent with pores in the mesoporous range of 2-25 nm as can be visualised on pore size distributions curves in figure 6.2. The desorption curves are practically coincide with adsorption branch of the respective sorption isotherms of all the samples irrespective of the composition of the catalysts. This behaviour is a representative of open textured pores, which offers practically negligible diffusion resistance during the reaction.

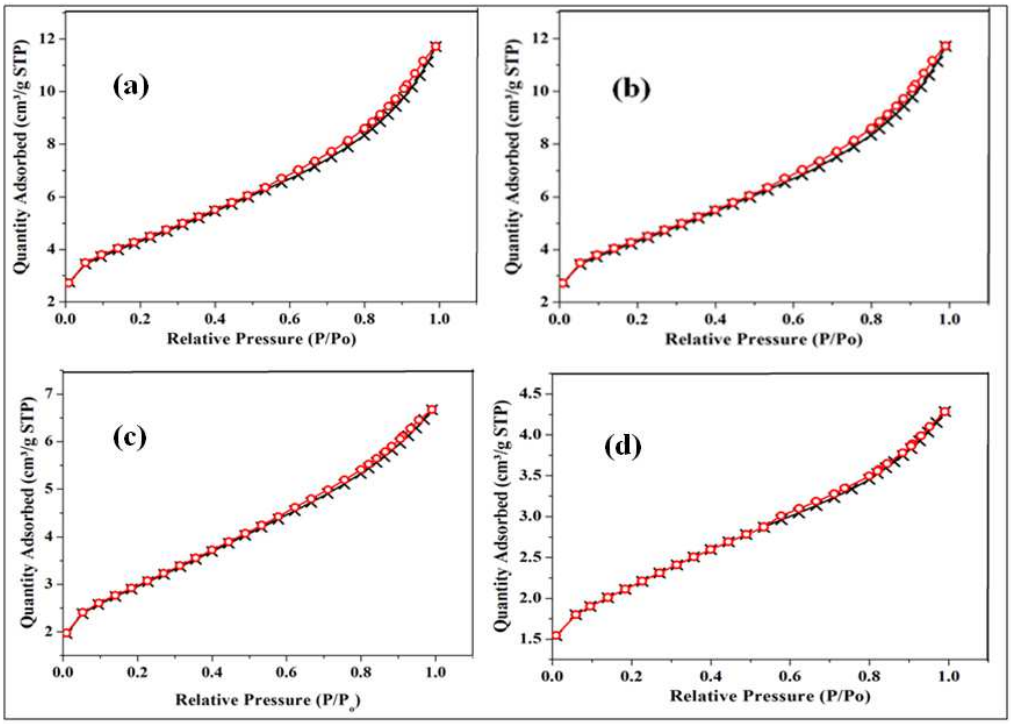


**Figure 6.1** $N_2$ Physisorption isotherms of catalysts (a) $La_{0.9}Sr_{0.1}CoO_3$, (b) $La_{0.9}Sr_{0.1}Co_{0.5}Ni_{0.5}O_{3-\delta}$, (c) $La_{0.9}Sr_{0.1}Co_{0.5}Cu_{0.5}O_{3-\delta}$ and (d) $La_{0.9}Sr_{0.1}Co_{0.5}Fe_{0.5}O_{3-\delta}$

The pore size distribution curves presented in figure 6.2 for $La_{0.9}Sr_{0.1}CoO_3$, $La_{0.9}Sr_{0.1}Co_{0.5}Cu_{0.5}O_{3-\delta}$ and $La_{0.9}Sr_{0.1}Co_{0.5}Fe_{0.5}O_{3-\delta}$ catalysts show similar trimodal nature while catalyst $La_{0.9}Sr_{0.1}Co_{0.5}Ni_{0.5}O_{3-\delta}$ displays monomodal with most probable pore around 70 Å. In the case of $La_{0.9}Sr_{0.1}CoO_3$, the most probable pores were found around 40, 140, 220 Å and, while in the case of $La_{0.9}Sr_{0.1}Co_{0.5}Cu_{0.5}O_{3-\delta}$ and $La_{0.9}Sr_{0.1}Co_{0.5}Fe_{0.5}O_{3-\delta}$ the first peak appeared around 40Å with others near 110 and 220 Å.

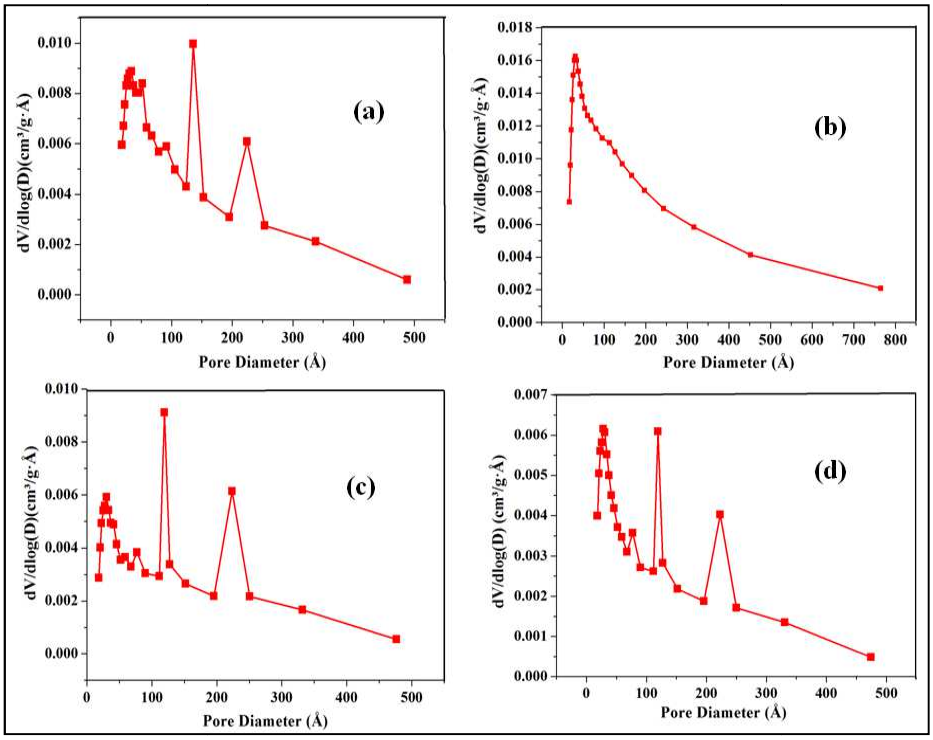


**Figure 6.2** Pore size distribution curves of catalysts (a) $La_{0.9}Sr_{0.1}CoO_3$, (b) $La_{0.9}Sr_{0.1}Co_{0.5}Ni_{0.5}O_{3-\delta}$, (c) $La_{0.9}Sr_{0.1}Co_{0.5}Cu_{0.5}O_{3-\delta}$ and (d) $La_{0.9}Sr_{0.1}Co_{0.5}Fe_{0.5}O_{3-\delta}$

The textural properties including BET surface area, total pore volume and average pore diameter of the perovskites studied in the present investigation are summarized in Table 6.1. It can be seen from the table that the various perovskite have low specific surface area (4.80-15 $m^2/g$), which is in expected range considering the high synthesis temperature in accordance with references [Russo et al.2008, Campagnoli et al. 2005]. The $La_{0.9}Sr_{0.1}Co_{0.5}Ni_{0.5}O_{3-\delta}$ sample calcined at 750$^oC$ in air showed the highest surface area (15.00 $m^2/g$). Similarly the catalyst $LaNiO_3$ calcined in air, displayed the lowest surface area (4.80 $m^2/g$). The catalyst $La_{0.9}Sr_{0.1}Co_{0.5}Cu_{0.5}O_{3-\delta}$ exhibited the lowest average pore diameter (06.18 Å) and comparable pore volume (0.0056 $cm^3/g$) with other catalysts. It can be seen from the table that on substitution of Sr and Fe in $LaCoO_3$, the surface area of the catalyst decreased to the value of 7.29 $m^2/g$.

**Table 6.1** Textural characterization of perovskite catalyst samples

| Catalyst | BET surface area ($m^2/g$) | Pore volume ($cm^3/g$) | Average pore dia.(Å) |
|---|---|---|---|
| $LaCoO_3$ | 09.12 | 0.0074 | 41.70 |
| $LaFeO_3$ | 07.91 | 0.0081 | 40.23 |
| $LaNiO_3$ | 04.80 | 0.0096 | 42.89 |
| $LaZnO_y$ | 05.87 | 0.0087 | 36.67 |
| $La_{0.9}Sr_{0.1}CoO_3$ | 10.14 | 0.0058 | 08.04 |
| $La_{0.9}Sr_{0.1}Co_{0.5}Ni_{0.5}O_{3-\delta}$ | 15.00 | 0.0088 | 09.10 |
| $La_{0.9}Sr_{0.1}Co_{0.5}Cu_{0.5}O_{3-\delta}$ | 07.55 | 0.0043 | 06.18 |
| $La_{0.9}Sr_{0.1}Co_{0.5}Fe_{0.5}O_{3-\delta}$ | 07.29 | 0.0056 | 06.51 |

### 6.3.2 XRD Characterization of pure and substituted catalysts

The powder XRD patterns of catalyst samples prepared by citric acid sol-gel method are shown in figure 6.3. The XRD peaks were found to be very sharp indicating that the $ABO_3$ perovskite structure is well maintained in all the prepared catalysts, Instead of expectation in Catalyst $LaZnO_y$, perovskite structure is totally inaccessible. In figure 6.3 the obtained XRD data were compared with the standard JCPDS pattern for $LaCoO_3$ (with JCPDS card No. 25-1060), $LaFeO_3$ (with JCPDS card no. 37-1493) and $LaNiO_3$ (with JCPDS card no.33-0711) while in $LaZnO_y$ shows the presence of $La_2O_3$ (with JCPDS card No. 83-1344), $La(OH)_3$ (with JCPDS card No. 83-2034) and ZnO (with JCPDS card No. 89-1397) as the main crystalline phase. Thus, $LaZnO_y$ does not form perovskite structure but the constituents are present in catalyst as the mixed oxides. The crystallite size was estimated using the Scherrer equation (3.9). The crystallite size data are reported in Table 6.2. The crystallite size values were found in the range of 14.52-33.50 nm. $LaNiO_3$ shows the smallest crystallite size of 14.52 nm, whereas; $LaCoO_3$ shows the largest crystallite size of 32.13 nm.

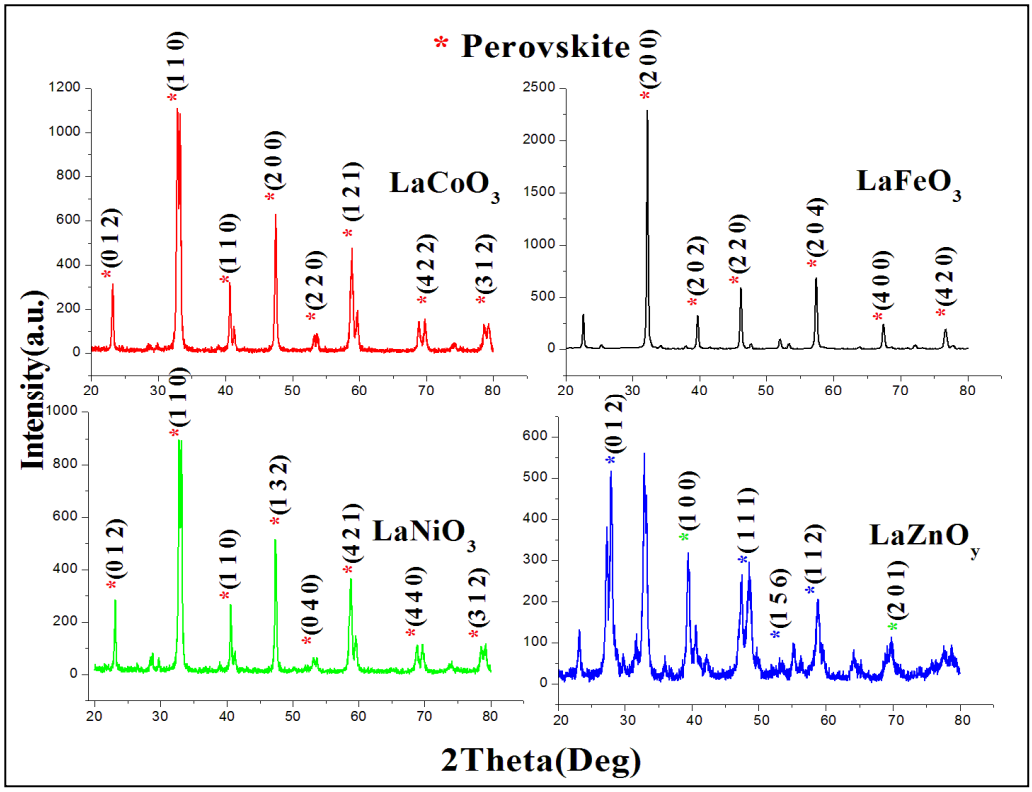


**Figure 6.3** XRD Pattern of (A) $LaCoO_3$, (B) $LaFeO_3$, (C) $LaNiO_3$ and (D) $LaZnO_y$

In Catalyst $LaZnO_y$ the presence of $La(OH)_3$ phase is very unusual as calcination of sol-gel precursors at 750°C decomposes lanthanum compounds purely into $La_2O_3$ according to following reactions (equation 6.1 & 6.2) [Peralta et al. 2011]:

$$La(OH)_3 \xrightarrow{300-400\ ^oC} LaOOH \xrightarrow{400-500\ ^oC} La_2O_3 \quad (6.1)$$

$$La_2O_2CO_3 \xrightarrow{400-460\ ^oC\ CO_2} La_2(CO_3)_3 \xrightarrow{460-550\ ^oC} La_2O_2CO_3 \xrightarrow{>600\ ^oC} La_2O_3 \quad (6.2)$$

However, presence of $La(OH)_3$ in the XRD diffractogram (figure 6.3(D)), may be due to exposure of the catalysts to ambient conditions favouring hydroxylation of $La_2O_3$.

The powder XRD patterns of substituted perovskite catalyst samples are shown in Figure 6.4. Since the standard XRD data for substituted catalyst samples is not

available in the literature, the obtained XRD data were compared with the XRD data of the standard JCPDS pattern for $LaCoO_3$ (JCPDS card No. 25-1060). In addition, the main diffraction peaks of the samples containing Sr shift to lower 2θ position as compared with pure $LaCoO_3$, evidencing that the relatively larger strontium ion has been incorporated into the perovskite structure. In $La_{0.9}Sr_{0.1}CoO_3$ and $La_{0.9}Sr_{0.1}Co_{0.5}Ni_{0.5}O_{3-\delta}$ a very weak peak at 2θ = 46.9◦ can be detected, suggesting that a small amount of $Co_3O_4$ may be present, as shown in Figure 6.4 for $La_{0.9}Sr_{0.1}Co_{0.5}Cu_{0.5}O_{3-\delta}$, the main diffraction peaks shift to lower 2θ position as compared with the other catalysts. This result implies that the relatively larger $Sr^{2+}$ and $Cu^{2+}$ ions have been successfully incorporated into the lattice of perovskite structure. The Fe-substitution in $La_{0.9}Sr_{0.1}Co_{0.5}Fe_{0.5}O_{3-\delta}$ increased the intensity of the main diffraction peaks indicates that Fe-substitution increases the degree of crystallization. It should also be noted that the Fe-substitution makes the main diffraction peaks shift to lower 2θ position, evidencing that the relatively large iron ion has been introduced into the perovskite structure. The crystallite size was estimated using the Scherrer equation (3.9) and are reported in Table 6.2.The crystallite size values were found in the range of 11.01-36.50 nm. Ni- substituted Catalyst shows the smallest crystallite size of 11.01 nm, whereas; the Cu-substituted, catalyst shows the largest crystallite size of 36.50 nm.

**Table 6.2** The crystallite size of all the catalysts

| **Catalyst** | **Crystallite size (nm)** | | |
|---|---|---|---|
| $LaCoO_3$ | 32.13 | | |
| $LaFeO_3$ | 25.12 | | |
| $LaNiO_3$ | 14.52 | | |
| $LaZnO_y$ | $La_2O_3$ | $La(OH)_3$ | ZnO |
| | 33.5 | 23 | 27.1 |
| $La_{0.9}Sr_{0.1}CoO_3$ | 14.71 | | |
| $La_{0.9}Sr_{0.1}Co_{0.5}Ni_{0.5}O_{3-\delta}$ | 11.01 | | |
| $La_{0.9}Sr_{0.1}Co_{0.5}Cu_{0.5}O_{3-\delta}$ | 36.5 | | |
| $La_{0.9}Sr_{0.1}Co_{0.5}Fe_{0.5}O_{3-\delta}$ | 14.09 | | |

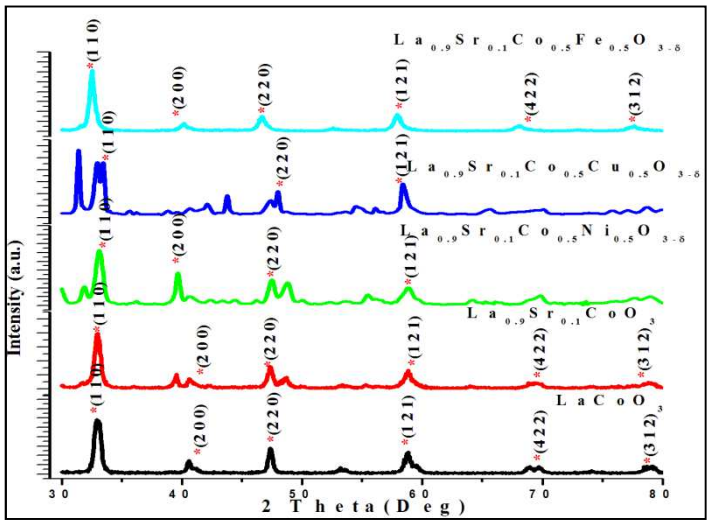


**Figure 6.4** XRD Pattern of Pure and Substituted Perovskite Catalysts

### 6.3.3 FTIR Characterization of Pure and Substituted Catalysts

The FTIR spectra in the range 4000-400cm$^{-1}$ of the catalysts prepared are shown in figure 6.5, 6.6 and 6.7. Figure 6.5 depicts the FTIR spectra of the pure perovskite catalysts ($LaCoO_3$, $LaFeO_3$ and $LaNiO_3$) calcined at the 750 $^oC$ in stagnant air. The broad absorption bands around 3020 cm$^{-1}$ and 2350 cm$^{-1}$ appeared in the IR spectra corresponded to OH stretching and OH bending of water. The absorption band near 1490 cm$^{-1}$ was corresponded to nitrate ion. In addition, the band at 1100 cm$^{-1}$ was corresponded to Co-OH bending which is confirmed with the reported value that MOH bending mode appears below 1200 cm$^{-1}$ [Nakamoto 1997]. The absorption band at ~ 600 cm$^{-1}$ are ascribed to Co-O / Fe-O /Ni-O and $MO_6$ stretch vibrations in the perovskite structure.

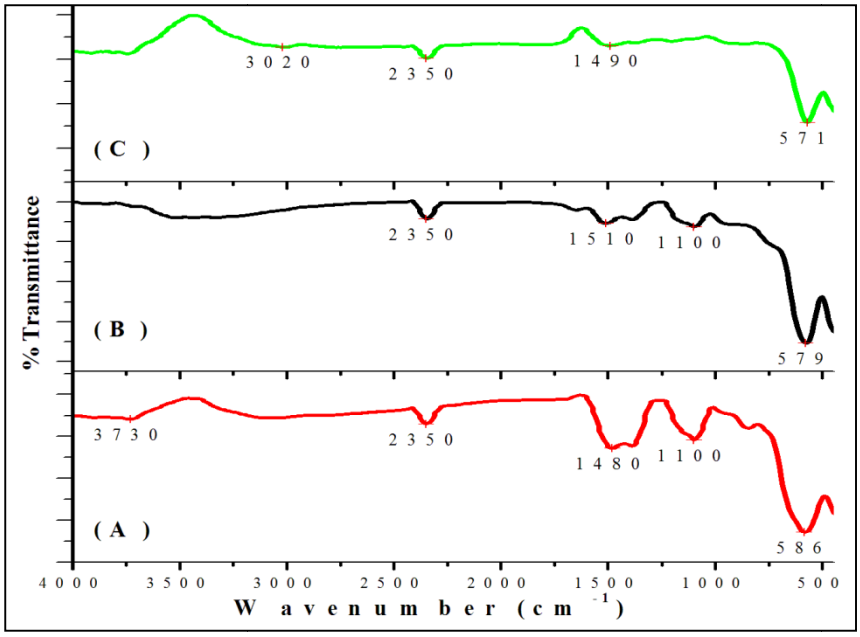


**Figure 6.5** FTIR spectra of (A) $LaCoO_3$, (B) $LaFeO_3$, (C) $LaNiO_3$

Figure 6.6 shows the FTIR spectra of $LaZnO_y$. An intense and sharp band at 3609.4 $cm^{-1}$ is assigned to the stretching and bending O–H vibrations of lanthanum hydroxide [Zhu et al. 2008]. Bands near 3444$cm^{-1}$ represent the O-H stretching mode indicative of the presence of adsorbed water on the sample surface [Zhu et al. 2007 ] and peaks at 1496 and 1385$cm^{-1}$ shows $La_2O_2CO_3$ [Mu and Wang 2011]. The strong peak at 1066 $cm^{-1}$ is assigned to the Zn–O–H bending. 538. 13$cm^{-1}$ and 656.29$cm^{-1}$ shows the characteristics peak of ZnO and $La_2O_3$ [Vasudevan et al. 2013].

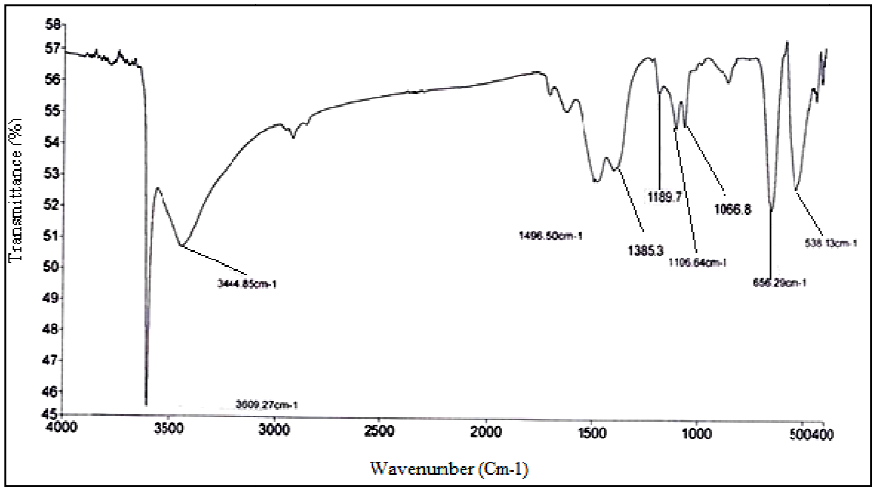


**Figure 6.6** FTIR spectra of the $LaZnO_y$

Figure 6.7 depicts the FTIR spectra of the substituted catalysts calcined at 750$^{o}$C in air. The broader peak appeared at ~590 cm$^{-1}$ is characteristic of the $MO_6$ octahedra commonly found in perovskite oxide powder and is observed in this system too [Ramesh et al. 1995]. The peaks found near to 2350 cm$^{-1}$ in the samples are due to the presence of atmospheric moisture as reported earlier [Mandelovici et al. 1994]. The absorption band at 1480, 1490 and 1500 cm$^{-1}$ was corresponded to nitrate ion. In addition, the band at 1100, 1200 ans 1210 cm$^{-1}$ was corresponded to Co-OH bending which is confirmed with the reported value that MOH bending mode appears below 1200 cm$^{-1}$ [Nakamoto 1997]. The absorption band at 586 and 594 cm$^{-1}$ in figure 6.7 related to Co-O stretching vibration, which was confirmed with the reported value that cobalt-oxygen stretching appears at around 600 cm$^{-1}$ [Khalil 2003].

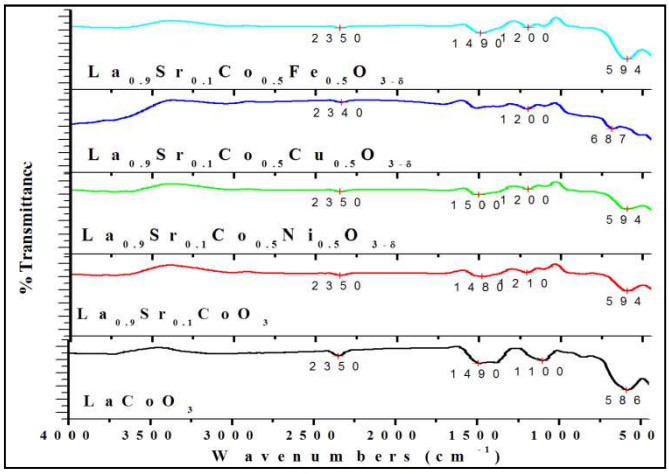


**Figure 6.7** FTIR spectra of Pure and Substituted Perovskite Catalysts

### 6.3.4 XPS Analysis of the Catalysts

X-ray photoelectron spectroscopy (XPS) has been done to confirm the oxidation state of the elements present in the samples. The characteristic spectra collected for La 3d, Co 2p Fe 2p, Ni 2p Cu 2p and O 1s in catalysts are displayed in Figures 6.8 to 6.13. In figure 6.8(a) the peaks of La $3d_{5/2}$ and La $3d_{3/2}$ were situated at 836.2 eV and 839.8 eV

and at 854.1 eV and 858.5 eV, respectively. The spin-orbit splitting of La 3d level is 18.7 eV. Fig. 6.8(b) shows the binding energies of the Co 2p main lines, it is difficult to determine the oxidation states of cobalt cations because similar values can be obtained for most of the cobalt oxides and hydroxides (e.g. CoO, $Co_2O_3$, $Co_3O_4$ and CoOOH). The spin-orbit splitting of Co 2p level is 15.2 eV which is similar to the reported value [Cesar et al. 2000] For $Co_3O_4$ with mixed valence of Co ions. The Co 2p XPS spectra of the catalysts consists of two main lines with the spin-orbit splitting (ΔE) falling in the range of $Co_3O_4$, implying that the cobalt ions exist in the mixed valence states of +2 and +3. As a result of high-valent Co ion, oxygen vacancies are created which accumulates a large number of adsorption oxygen on the surface. The O 1s energy spectrum consists of two peaks, which correspond to two forms of oxygen, i.e. lattice oxygen $O_{lat}$ and adsorption oxygen $O_{ads}$ on the sample surface (fig. 6.8C). The peak at the binding energy of 530.5 eV corresponds to the lattice oxygen species ($O^{2-}$, $O^{-}$), which reflect the redox behavior of the metal, and the peak at 532.8 eV corresponds to the adsorption oxygen species ($O_2^{-}$, $O_2^{2-}$), which is the active centre for the oxidation [Zhao et al. 1996, Wang et al 2012].

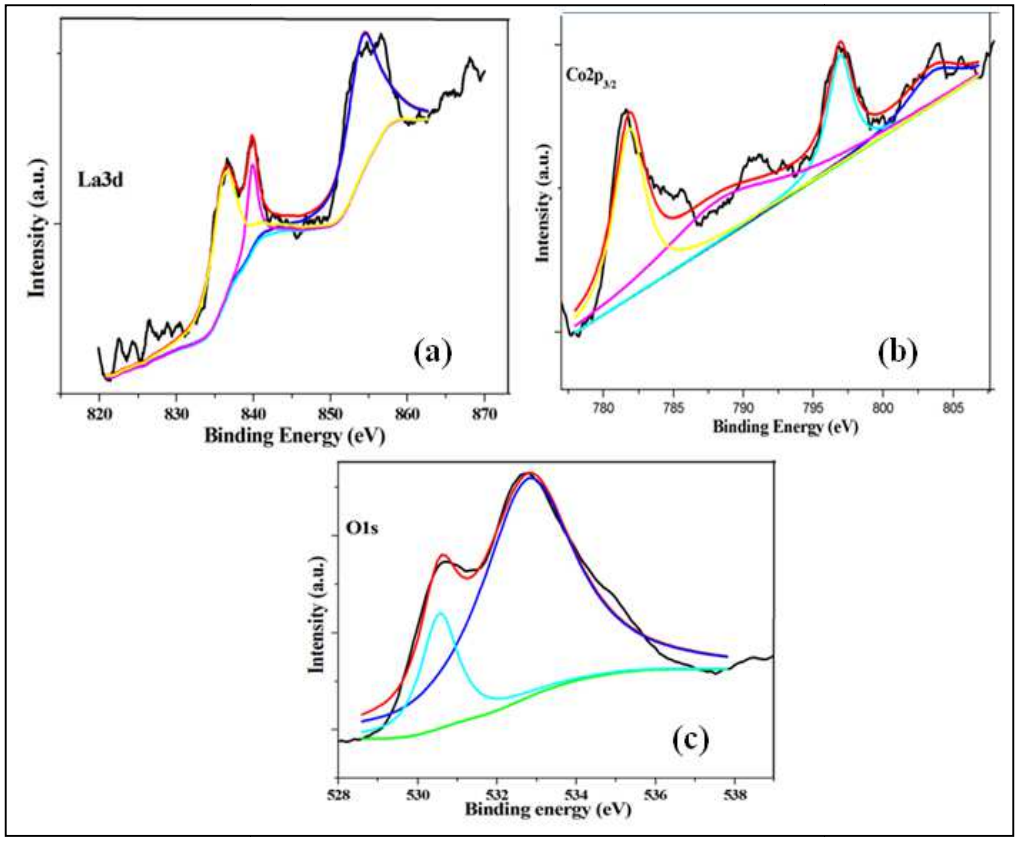


**Figure 6.8** XPS Spectra of $LaCoO_3$

Figure 6.9 displays the XPS spectra of La 3d, Fe 2p and O 1s for $LaFeO_3$. In Figure 6.9(a) the peaks of La $3d_{5/2}$ and La $3d_{3/2}$ were situated at 838.2 eV and 841.2 eV and at 855.6 eV and 859.0 eV, respectively. The spin-orbit splitting of La 3d level is 17.4 eV. In Figure 6.9 (b), the peaks at 714.6 and 727.4 eV correspond to the binding energies of Fe $2p_{3/2}$ and $2p_{1/2}$, respectively [Parida et al. 2010]. No *noticeable* shoulder peaks are found in the Fe 2p XPS spectrum, indicating that Fe mainly exhibits +3 oxidation states. The broad and asymmetric O1s XPS spectra (figure 6.9c) at binding energies of 533.0 and 535.3 eV correspond to the lattice oxygen species and the adsorption oxygen species respectively.

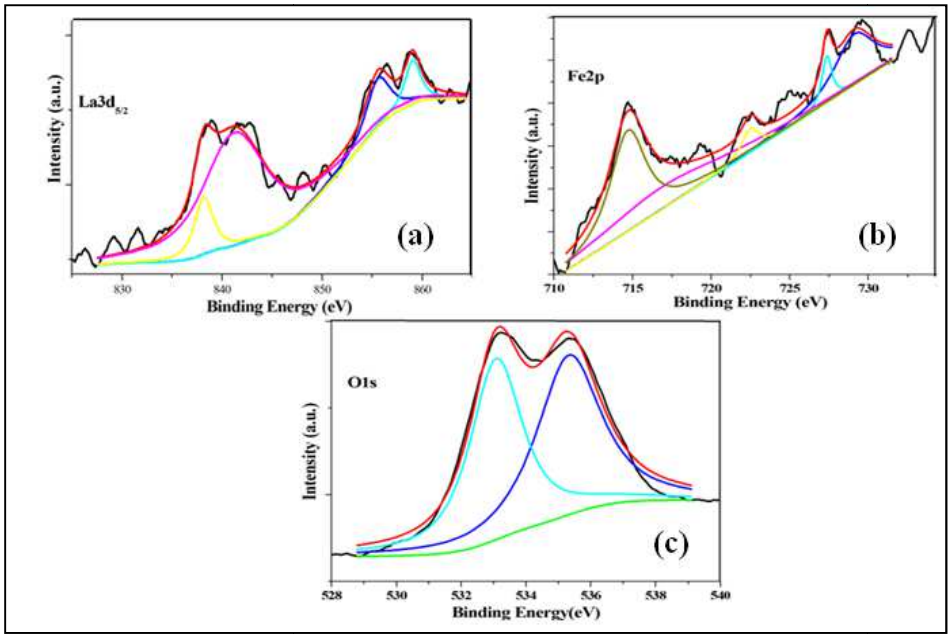


**Figure 6.9** XPS Spectra of $LaFeO_3$

Figure 6.10 shows the XPS spectra of La 3d, Co 2p and O 1s for $La_{0.9}Sr_{0.1}CoO_3$. The peaks of La $3d_{5/2}$ and La $3d_{3/2}$ were situated at 839.1 and 856.5 eV, respectively. The spin-orbit splitting of La 3d level is 17.3 eV. In Figure 6.10 (b), the peaks at 782.9 eV correspond to the binding energies of $Co2p_{3/2}$ [Parida et al. 2010]. The broad O1s XPS spectra (figure 6.10c) at binding energies of 533.6 eV correspond to the adsorption oxygen species. Figure 6.11 shows the XPS Spectra of partial substitution of $La^{3+}$ by $Sr^{+}$ and Co by Ni in the $LaCoO_3$. The peaks of La $3d_{5/2}$ and La $3d_{3/2}$ were situated at 839.1 and 856.5 eV, respectively. The spin-orbit splitting of La 3d level is 17.3 eV. In figure 6.11 (b), the peak at 782.9 eV correspond to the binding energies of $Co2p_{3/2}$ [Parida et al. 2010]. In figure 6.11 (c) the peaks at 856.5 and 852.7 correspond to the binding energies of $Ni2p_{3/2}$. The broad and asymmetric O1s XPS spectra (figure 6.11c) at binding energies of 530.2 and 532.6 eV correspond to the lattice oxygen species and the adsorption oxygen species respectively.

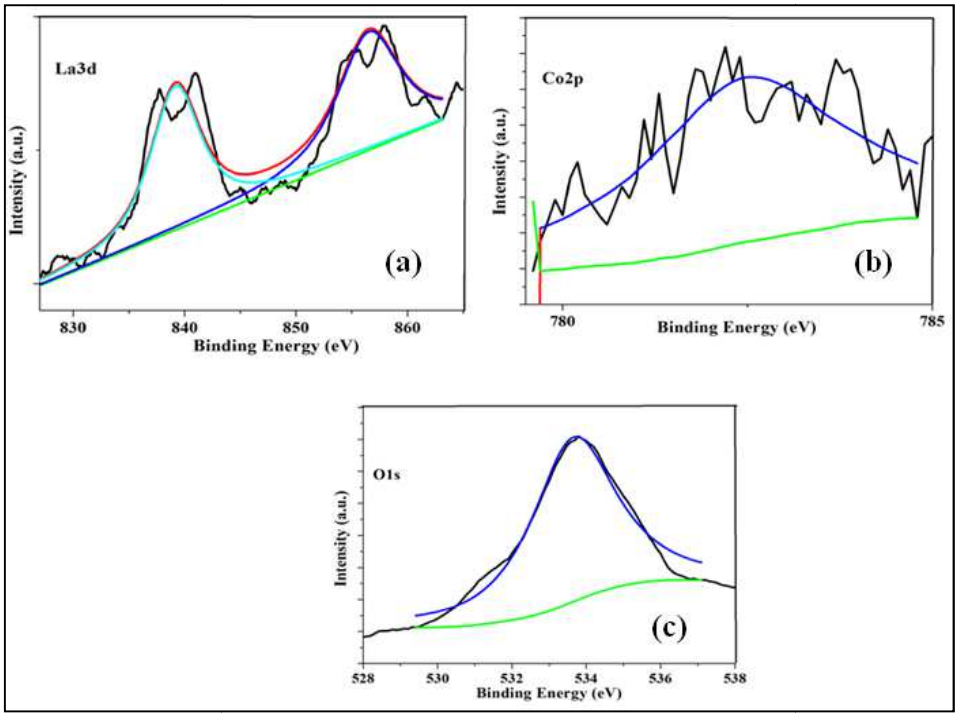


**Figure 6.10** XPS Spectra of $La_{0.9}Sr_{0.1}CoO_3$

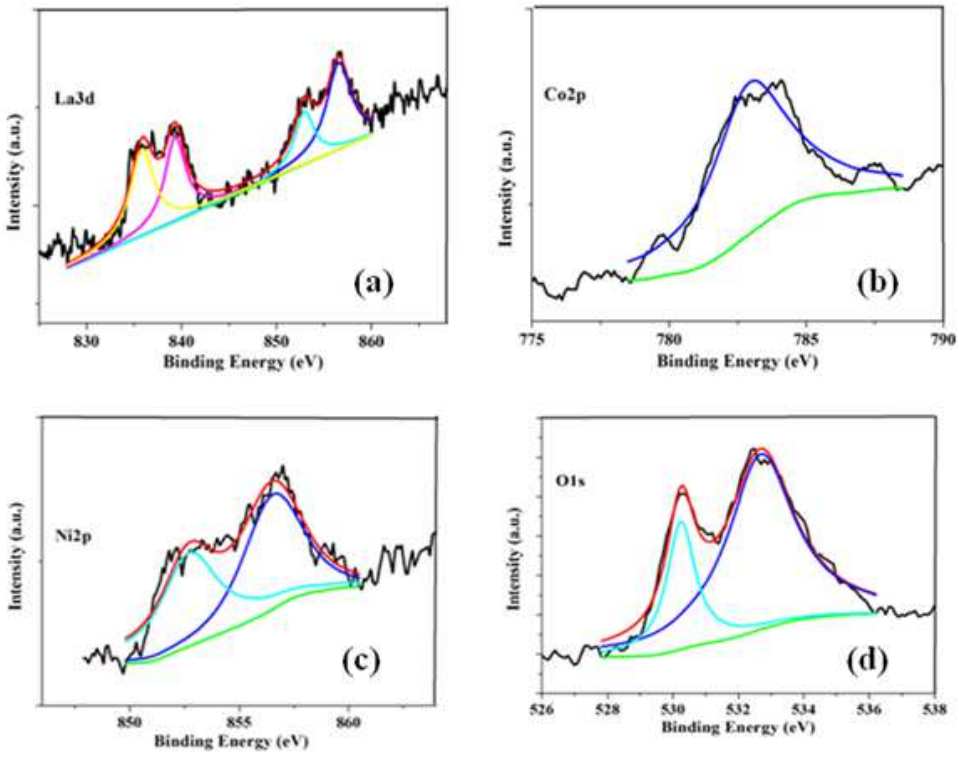


**Figure 6.11** XPS Spectra of $La_{0.9}Sr_{0.1}Co_{0.5}Ni_{0.5}O_{3-\delta}$

Figure 6.12 shows the XPS Spectra of partial substitution of $La^{3+}$ by $Sr^{+}$ and Co by Cu in the $LaCoO_3$ sample. The peaks of La $3d_{5/2}$ and La $3d_{3/2}$ were situated at 837.9 and

855.3 eV, respectively. The spin-orbit splitting of La 3d level is 16.4 eV. In figure 6.12 (b), the peak at 783.9 eV correspond to the binding energies of $Co2p_{3/2}$ [Parida et al. 2010]. In figure 6.12 (c) the peak at 711.9 correspond to the binding energies of Fe $2p_{3/2}$. The broad and asymmetric O1s XPS spectra (figure 6.12c) at binding energies of 530.5 and 533.1 eV correspond to the lattice oxygen species and the adsorption oxygen species respectively.

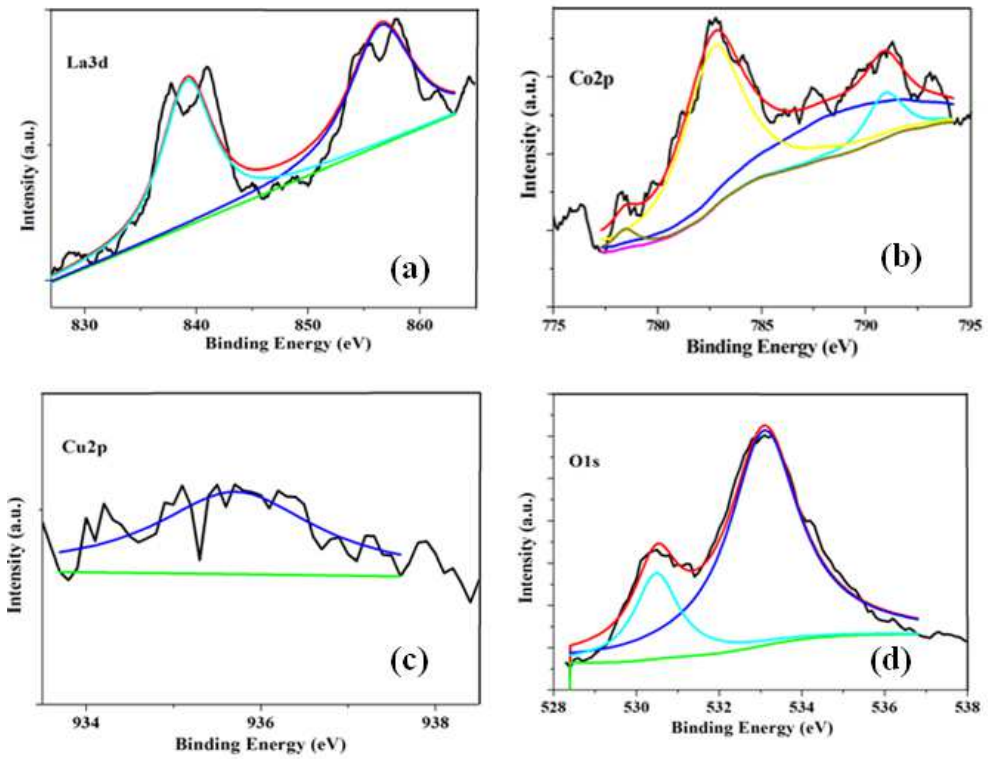


**Figure 6.12** XPS Spectra of $La_{0.9}Sr_{0.1}Co_{0.5}Cu_{0.5}O_{3-\delta}$

Figure 6.13 shows the XPS Spectra of partial substitution of $La^{3+}$ by $Sr^{+}$ and Co by Fe in the $LaCoO_3$ sample. There exists relatively more adsorption oxygen on the surface indicating the presence of more oxygen vacancies. These adsorption oxygen traps electron and form more active $O_2^-$. Figure 6.13(a) shows the XPS spectra of La 3d, the peaks of La $3d_{5/2}$ and La $3d_{3/2}$ were situated at 854.2 eV and 857.4 eV and at 837.1 eV and 840.6 eV, respectively. The spin-orbit splitting of La 3d level is 17.0 eV. Figure

6.13(b) and 6.13(c) shows the XPS spectra of Co 2p and Fe 2p respectively. The spin-orbit splitting of Co 2p and Fe 2p levels are 15.2 and 12.8 eV which is in well support with the literature. The O 1s energy spectrum consists of two peaks having binding energies 531.2 and 533.8, which correspond to two forms of oxygen, i.e. lattice oxygen and adsorption oxygen are shown in figure 6.13(d). As in this catalyst some of $La^{3+}$ was replaced by $Sr^{+}$, there were changes in the relative ratio of adsorption to lattice oxygen. More adsorption oxygen existed on the surface indicating the presence of more oxygen vacancies and an increased content of quasi-free electrons in the catalyst. More adsorption oxygen traps more electrons and thus it is favourable for forming more $O^{2-}$, which becomes more active centers for oxidation, thus it results in the enhancement in oxidizing ability of the catalyst. It would contribute to the decrease of the combustion temperature of soot particles.

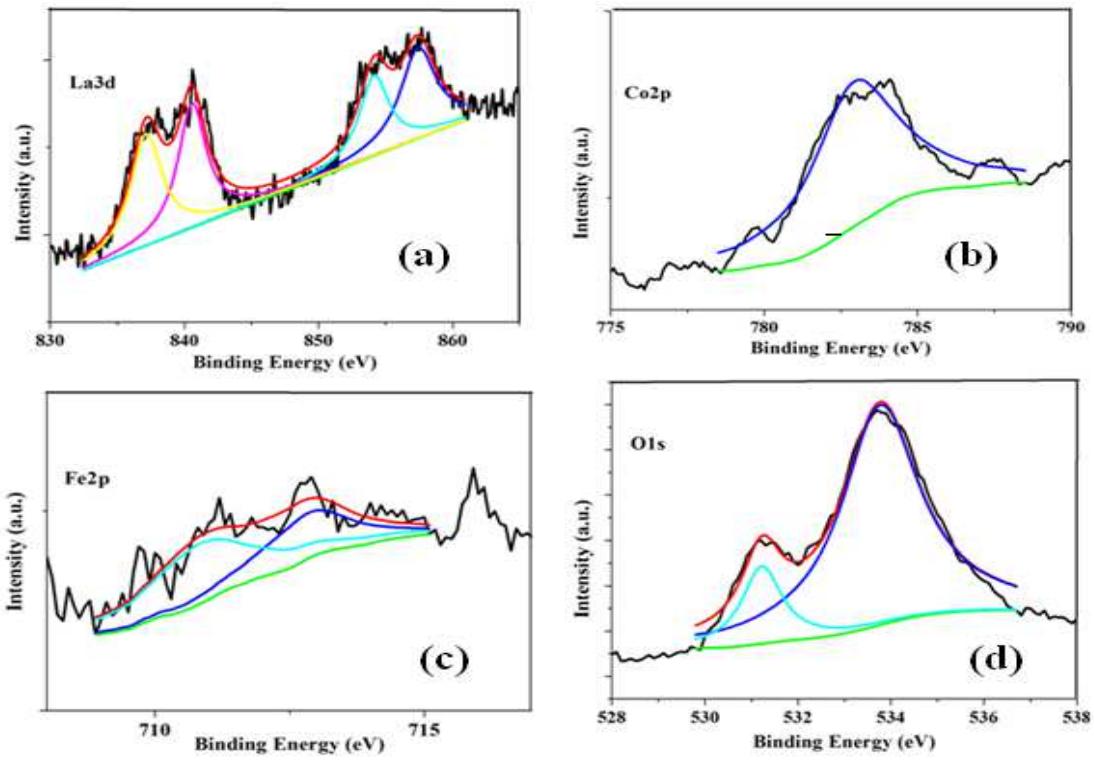


**Figure 6.13** XPS Spectra of $La_{0.9}Sr_{0.1}Co_{0.5}Fe_{0.5}O_{3-\delta}$

### 6.3.5 SEM characterization of the catalysts

The SEM micrographs of LaZnOy at different magnifications shown in figure 6.14 revealed that the prepared catalyst sample was highly porous, less aggregated and surface of the catalyst appears to be spongy tendrils. The particle size of the mixed oxides is small and uniformly distributed. The SEM images (figure 6.15) clearly show the difference in surface morphology due to presence of different B-site ions (Co, Fe and Ni). In comparison to $LaCoO_3$ other two perovskite ($LaFeO_3$ and $LaNiO_3$) were more aggregated and porus surface can be visualized (fig. 6.15F & G).

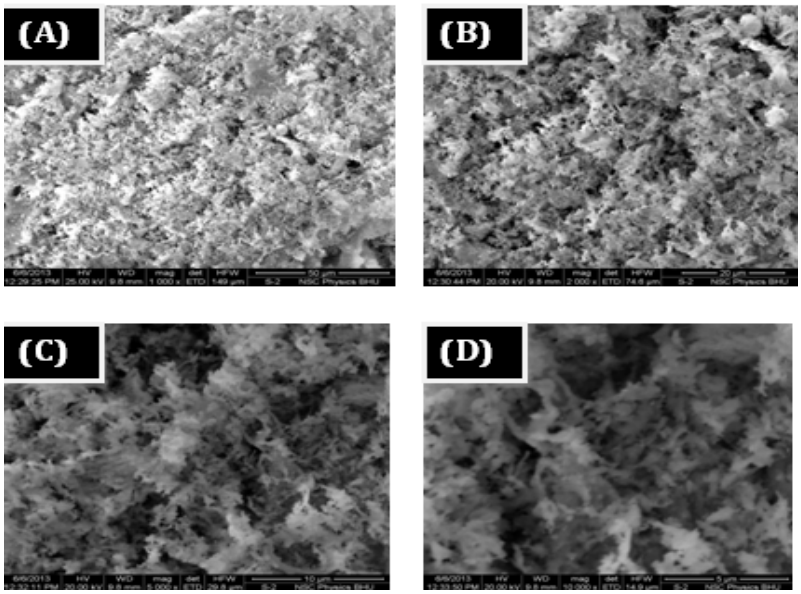


**Figure 6.14** SEM images of $LaZnO_y$ catalyst; (A) 1000x (B) 2,000x (C) 5,000x and (D) 10,000x magnification

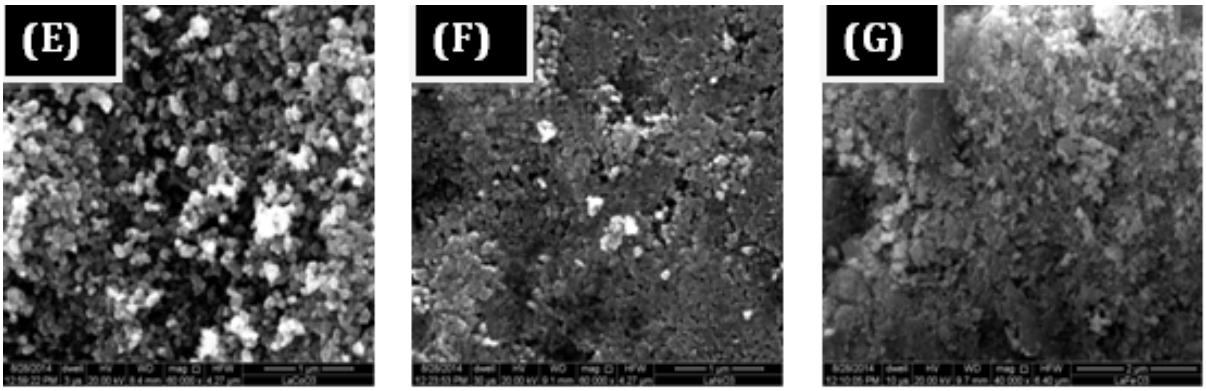


**Figure 6.15** SEM images of (E) $LaCoO_3$,(F) $LaFeO_3$, (G) $LaNiO_3$

It can be seen from figure 6.16 that the morphologies of particles are of irregular shape and within the nanoscale (<100 nm). The SEM images clearly show the difference in surface morphology by partial substitution of ions. When part of lanthanum ions in $LaCoO_3$ was partially substituted by Sr, more aggregated porous surface can be visualized. Further, substitution of cobalt ions in $La_{0.9}Sr_{0.1}CoO_3$ by Fe ions entirely different surface structure can be seen in figure 6.16(K) in comparison to figure 6.16(H & I). Morphological microscopy of the explored samples also demonstrated agglomerates involved mostly thin, smooth flakes and layers perforated by a large number of pores.

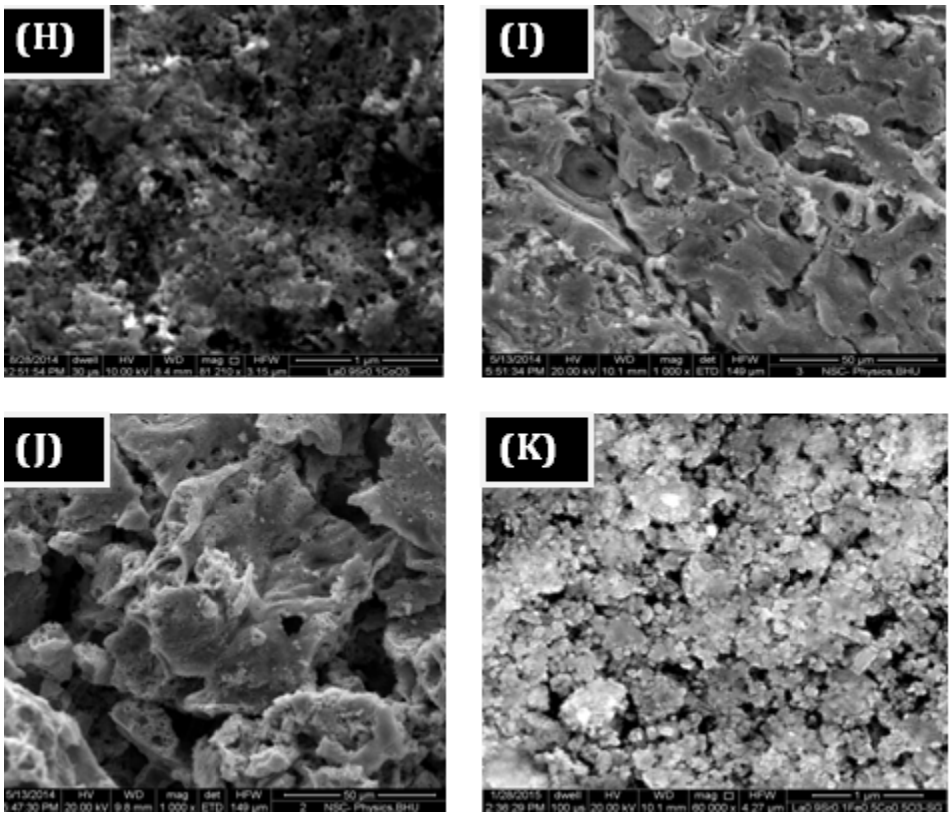


**Figure 6.16** SEM images of (H) $La_{0.9}Sr_{0.1}CoO_3$, (I) $La_{0.9}Sr_{0.1}Co_{0.5}Ni_{0.5}O_{3-\delta}$, (J) $La_{0.9}Sr_{0.1}Co_{0.5}Cu_{0.5}O_{3-\delta}$ and (K) $La_{0.9}Sr_{0.1}Co_{0.5}Fe_{0.5}O_{3-\delta}$

### 6.3.6 Activity evaluation of catalysts

The catalytic combustion tests of diesel soot were performed with an air flow rate of 150 ml//min over the catalyst samples prepared by sol-gel method as a function of temperature. The reproducibility of the experimental data was confirmed by repeating some of the tests for at least twice. Activity of the catalyst for soot oxidation was evaluated on the basis of light off temperature characteristics $T_i$, $T_{50}$ and $T_f$ where, $T_i$, $T_{50}$ and $T_f$ are temperature corresponding to the start of soot ignition, the 50% conversion of soot and total oxidation of soot respectively. Experiments for the soot oxidation were planned to run up-to maximum temperature of 450$^o$C which can be achieved by the diesel exhaust.

The first series of experiments were conducted to see the effect of transition metal Ni, Co, Fe, and Zn at the B-site of the $ABO_3$ perovskite on soot oxidation. Four catalysts $LaCoO_3$, $LaNiO_3$, $LaFeO_3$ and $LaZnO_y$ were tested for soot oxidation. The results of soot oxidation are shown in figure 6.17 and table 6.3 presents the light of characteritics. It can be seen from the figure that the oxidation of diesel soot over different catalyst $LaNiO_3$, $LaFeO_3$, $LaCoO_3$ and $LaZnO_y$ initiated at different temperatures of 290, 319, 336 and 376$^o$C respectively. Similarly, the temperature for total oxidation of the soot over different catalyst $LaNiO_3$, $LaFeO_3$, $LaCoO_3$ and $LaZnO_y$ were 441, 428, 420 and 456$^o$C respectively. Except $LaZnO_y$ catalyst, all other catalysts showed total combustion of the soot < 450$^o$C, i.e. within the temperature window of diesel exhaust. It is can be concluded from the results reported in the figure and the table that $LaCoO_3$ catalyst is the best for soot oxidation under the present experimental conditions. The catalytic activity of the catalyst samples chiefly depends on three factors: chemical composition, degree of crystallinity, and the crystals morphology.

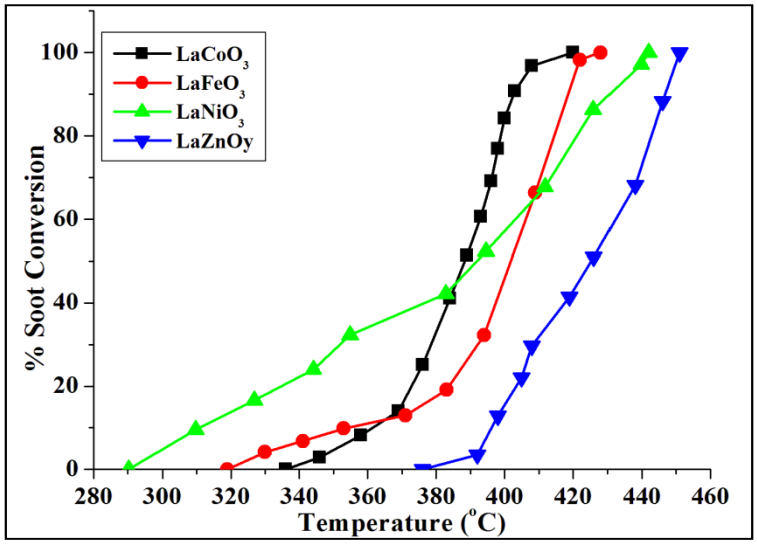


**Figure 6.17** Soot conversion over Perovskite-type Catalysts, Calcined at 750 $^{o}$C, Catalyst/ Soot: 10/1, Tight Contact, Air flow rate: 150ml/min

**Table 6.3** Light off Characteristics Temperatures of Perovskite-Type Catalysts

| Catalysts | $T_i$($^{o}$C) | $T_{50}$($^{o}$C) | $T_f$($^{o}$C) |
|---|---|---|---|
| $LaCoO_3$ | 336 | 389 | 420 |
| $LaFeO_3$ | 319 | 397 | 428 |
| $LaNiO_3$ | 290 | 392 | 441 |
| $LaZnO_y$ | 376 | 426 | 456 |

The second series of activity evaluation of catalysts were performed to optimize the value of "x" in $La_{1-x}Sr_xCoO_3$. Three catalysts $La_{1-x}Sr_xCoO_3$ (x = 0.1, 0.2, 0.3) were tested for soot oxidation. Figure 6.18 and table 6.4 shows that $La_{0.9}Sr_{0.1}CoO_3$ composition showed the highest activity for soot oxidation at $T_f$ = 416$^{o}$C. The optimum value of x in single substituted Sr-perovskite catalyst is found to be 0.1. However, the variation in catalyst activity in all the Sr substituted perovskite is very nominal. Thus, the substitution of Sr does not greatly affect the activity of the catalyst while it provides the stability to the catalyst as evidenced in table 6.5.

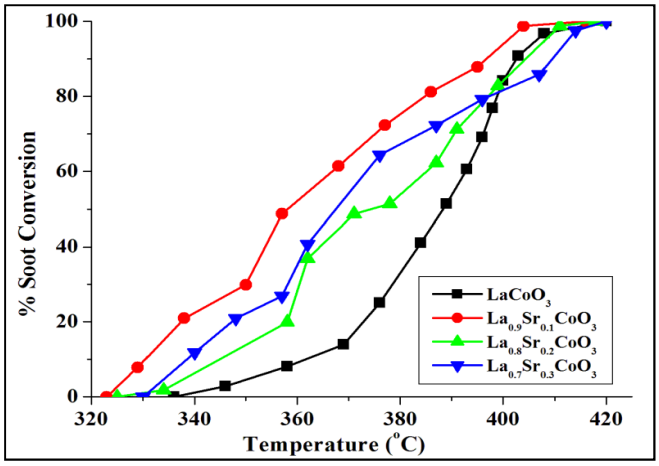


**Figure 6.18** Soot conversion over Single Sr-substituted Perovskite-type Catalysts, Calcined at 750 °C, Catalyst/ Soot: 10/1, Tight Contact, Air flow rate: 150ml/min

**Table 6.4** Light off characteristic temperatures of single Sr-substituted Perovskite-Type Catalysts

| Catalysts | $T_i$(°C) | $T_{50}$(°C) | $T_f$(°C) |
|---|---|---|---|
| $LaCoO_3$ | 336 | 389 | 420 |
| $La_{0.9}Sr_{0.1}CoO_3$ | 323 | 357 | 416 |
| $La_{0.8}Sr_{0.2}CoO_3$ | 325 | 371 | 418 |
| $La_{0.7}Sr_{0.3}CoO_3$ | 330 | 376 | 420 |

**Table 6.5** Stability test of catalyst $La_{0.9}Sr_{0.1}CoO_3$ for soot combustion under tight contact

| **Test Cycle** | **$T_i$(°C)** | **$T_{50}$(°C)** | **$T_f$(°C)** |
|---|---|---|---|
| 1st | 323 | 357 | 416 |
| 2nd | 322 | 357 | 417 |
| 3rd | 323 | 355 | 416 |
| 4th | 324 | 356 | 416 |
| 5th | 323 | 355 | 415 |

The previous observation showed that the optimum formulation of single substituted perovskite catalyst is $La_{0.9}Sr_{0.1}CoO_3$. Further, substitution of Co in $La_{0.9}Sr_{0.1}Co_{0.5}M_{0.5}O_3$

(M = Ni, Cu and Fe) were studied to find out the highly active promoter in double substituted perovskite catalyst. The soot oxidation studies performed over double substituted perovskites are shown in figure 6.19 and light off characteristics are given in table 6.6. The gradual increase in the activity was observed with substitution of Ni, Cu and Fe respectively and the enhancement of activity by double substitution of perovskite by promoter can be arranged in the following order: Fe > Cu > Ni. The improvement in activities due to substitution of Ni and Cu are marginal over $La_{0.9}Sr_{0.1}CoO_3$. From figure 6.19 and table 6.6 it can be concluded that the best formulation of double substituted perovskite is $La_{0.9}Sr_{0.1}Co_{0.5}Fe_{0.5}O_3$.

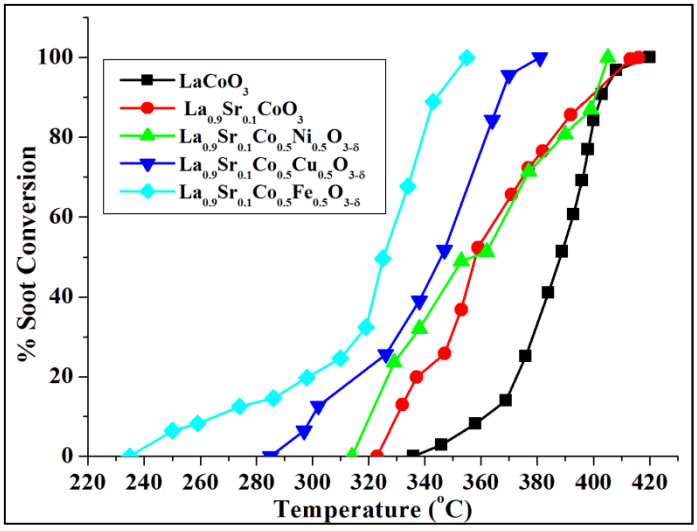


**Figure 6.19** Soot conversion over Substituted Perovskite-type Catalysts, Calcined at 750 $^{o}$C, Catalyst/ Soot: 10/1, Tight Contact, Air flow rate: 150ml/min

**Table 6.6** Characteristic lights off temperature for soot oxidation over perovskite catalysts

| Catalyst | $T_i$($^{o}$C) | $T_{50}$($^{o}$C) | $T_f$($^{o}$C) |
|---|---|---|---|
| $LaCoO_3$ | 336 | 389 | 420 |
| $La_{0.9}Sr_{0.1}CoO_3$ | 323 | 357 | 416 |
| $La_{0.9}Sr_{0.1}Co_{0.5}Ni_{0.5}O_{3-\delta}$ | 317 | 369 | 402 |
| $La_{0.9}Sr_{0.1}Co_{0.5}Cu_{0.5}O_{3-\delta}$ | 285 | 350 | 381 |
| $La_{0.9}Sr_{0.1}Co_{0.5}Fe_{0.5}O_{3-\delta}$ | 238 | 330 | 355 |

### 6.3.7 Effect of Gas Hourly space Velocity (GHSV) on Soot Oxidation

Experiments were conducted to optimize the flow rate of air from 50-200 ml/min or GHSV 7520-30080 $h^{-1}$ on soot oxidation over $La_{0.9}Sr_{0.1}Co_{0.5}Fe_{0.5}O_{3-\delta}$. Figure 6.20 shows that increasing GHSV 7520 $h^{-1}$ to 22560 $h^{-1}$ caused decrease in the characteristic temperatures ($T_i$, $T_{50}$, $T_f$) while further increase in flow rate to 30080 $h^{-1}$ increased the characteristic temperatures. This phenomenon explains two counter effects of increasing GHSV on soot oxidation. Increasing flow rate of air led to more oxidants ($O_2$), which helps to improve the combustion of soot particle. On the other hand increase in the air flow rate shortened the contact time of the reactants which negatively affect the soot oxidation. These two counter affects gave optimum value of GHSV at 22560 $h^{-1}$ showing lowest characteristic temperatures ($T_i$ = 238°C, $T_{50}$=330°C and $T_f$=355°C). Table 6.7 shows characteristic temperatures of soot oxidation at different GHSV.

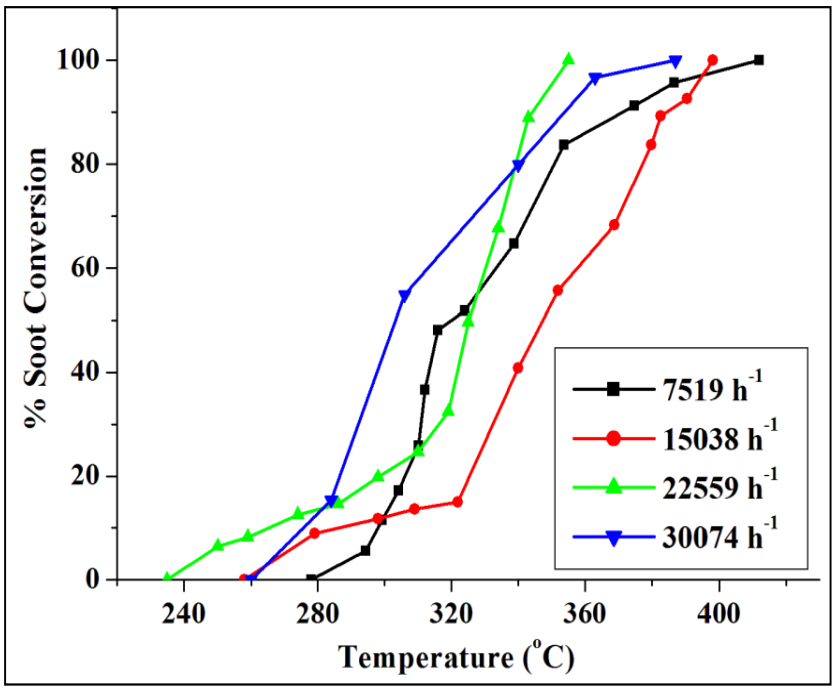


**Figure 6.20** Effect of Gas Hourly space Velocity on soot oxidation, by $La_{0.9}Sr_{0.1}Co_{0.5}Fe_{0.5}O_{3-\delta}$, (Catalyst/Soot: 10/1)

**Table 6.7** Characteristic temperature of soot oxidation over $La_{0.9}Sr_{0.1}Co_{0.5}Fe_{0.5}O_{3-\delta}$ at different space velocities

| GHSV ($h^{-1}$) | $T_i$($^oC$) | $T_{50}$($^oC$) | $T_f$($^oC$) |
|---|---|---|---|
| 7520 | 278 | 368 | 412 |
| 15040 | 258 | 354 | 398 |
| 22560 | 238 | 330 | 355 |
| 30080 | 260 | 356 | 387 |

### 6.3.8 Effect of Catalyst-Soot Contact

A loose contact study was also carried out to simulate the actual circumstances of diesel particulate filter (Guillen-hurtado et al. 2014). Figure 6.21 shows a comparison of conversion of soot particles over $La_{0.9}Sr_{0.1}Co_{0.5}Fe_{0.5}O_{3-\delta}$ under tight and loose contacts conditions of the catalyst-soot. It can be visualized from figure 6.21 that loose contact exhibited lower activity than tight contact. The observation is obvious as the catalysis is a surface phenomenon, higher the surface contacts (tight contact) higher the activity. From the table 6.7 it is clear that $La_{0.9}Sr_{0.1}Co_{0.5}Fe_{0.5}O_{3-\delta}$ resulted complete soot oxidation at $T_f$ = 407$^oC$ under loose contact which is 52$^oC$ higher than tight contact. The catalytic activity for soot oxidation under loose contact conditions is found to be very much appreciating within the diesel exhaust conditions i.e. < 450$^oC$. Thus, it should be effective to oxidize the soot on coating over DPF in real diesel engine exhaust.

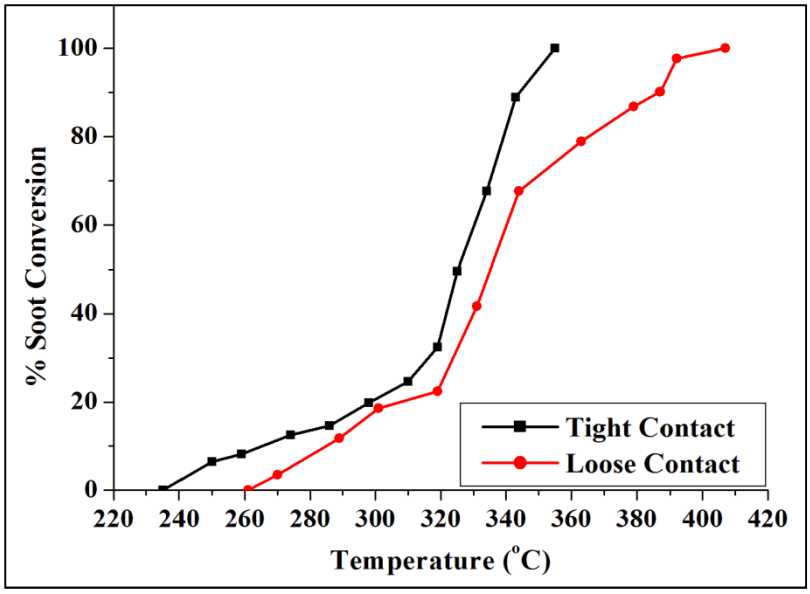


**Figure 6.21** Effect of contact type on soot oxidation on $La_{0.9}Sr_{0.1}Co_{0.5}Fe_{0.5}O_{3-\delta}$ catalyst, Calcination 750°C Catalyst/Soot: 10/1, air flow rate: 150ml/min

**Table 6.8** Effect of contact type on soot oxidation on $La_{0.9}Sr_{0.1}Co_{0.5}Fe_{0.5}O_{3-\delta}$ catalyst

| Contact condition | $T_i$(°C) | $T_{50}$(°C) | $T_f$(°C) |
|---|---|---|---|
| Tight contact | 238 | 330 | 355 |
| Loose contact | 261 | 349 | 407 |

### 6.3.9 Activity comparison of $La_{0.9}Sr_{0.1}Co_{0.5}Fe_{0.5}O_{3-\delta}$ with $La_{0.95}Pd_{0.05}Co_{0.5}Fe_{0.5}O_3$ catalyst for soot oxidation

Experiments were also performed to compare the catalytic activity for diesel soot oxidation with noble metal substituted perovskite catalyst. In literature it is reported that the best formulation of Pd-substituted perovskite as $La_{0.95}Pd_{0.05}Co_{0.5}Fe_{0.5}O_3$ for the soot oxidation**.** Therefore, the same composition of the catalyst was selected for comparative studies with optimized double substituted perovskite catalyst in the present work. The comparative results are shown in figure 6.22 as well as in table 6.9. It can be seen from the figure that in the beginning there was slow and gradual increase in soot conversion upto 430°C followed by sudden increase in conversion over noble metal substituted perovskite catalyst, reaching the total soot conversion at 499°C. Whereas,

for Sr-substituted perovskite catalyst the rate of soot conversion was faster from the very beginning in comparison to Pd-substituted catalyst. The complete combustion of soot over $La_{0.9}Sr_{0.1}Co_{0.5}Fe_{0.5}O_{3-\delta}$ occurred 144°C less than $La_{0.95}Pd_{0.05}Co_{0.5}Fe_{0.5}O_{3-\delta}$ catalyst. It is very evident from the light off characteristics data in table 6.9 and figure 6.22 that the activity of Sr-substituted perovskite is far better than Pd-substituted catalyst.

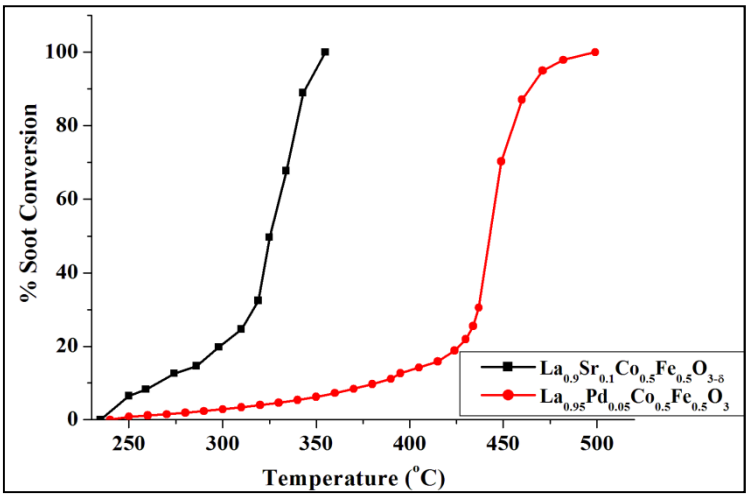


**Figure 6.22** Comparison of soot conversion over transition metal and noble metal based Perovskite-type Catalysts

**Table 6.9** Characteristic lights off temperature for soot oxidation over perovskite catalysts

| Catalyst | $T_i$(°C) | $T_{50}$(°C) | $T_f$(°C) |
|---|---|---|---|
| $La_{0.9}Sr_{0.1}Co_{0.5}Fe_{0.5}O_{3-\delta}$ | 238 | 330 | 355 |
| $La_{0.95}Pd_{0.05}Co_{0.5}Fe_{0.5}O_3$ | 241 | 442 | 499 |

## 6.4 Conclusions

Un-substituted $LaCoO_3$, $LaFeO_3$ and $LaNiO_3$; single substituted $La_{0.9}Sr_{0.1}CoO_3$ and double substituted $La_{0.9}Sr_{0.1}Co_{0.5}M_{0.5}O_{3-\delta}$ (where M= Fe, Ni and Cu) are synthesized by the sol-gel method. XRD analysis confirms the perovskite structure in all the prepared catalysts consisting of nano-size crystallites, whereas, $LaZnO_y$ catalyst is a mixture of metal oxides as confirmed by XRD and FTIR. Single substituted catalyst formulation,

$La_{0.9}Sr_{0.1}CoO_3$ shows better activity for the diesel soot oxidation than un-substituted $LaCoO_3$ perovskite.

The optimum composition of the double substituted catalyst resulted by calcination in air is $La_{0.9}Sr_{0.1}Co_{0.5}Fe_{0.5}O_{3-\delta}$ for soot oxidation which reveals the lowest temperature ($T_f$= 355$^oC$) for total soot oxidation amongst all the catalysts. The high catalytic activity of Fe-substituted perovskite catalysts can be elucidated from following aspects: firstly, the catalysts and the soot particulates fall in the nano-metric size range, ensuring a high contacting efficiency between soot particles and catalysts; secondly, the oxygen vacancies created by partial substitution of the perovskite structure confirmed by the XPS analysis, increases the oxidation ability of the catalysts. Optimum GHSV of 22560 $h^{-1}$ is found by experiment. Under the loose contact study performed on $La_{0.9}Sr_{0.1}Co_{0.5}Fe_{0.5}O_{3-\delta}$ shows an increase of $T_f$ by 52$^oC$ for oxidation of soot. The activity order of the catalyst in decreasing sequence for diesel soot oxidation is as follows: $La_{0.9}Sr_{0.1}Co_{0.5}Fe_{0.5}O_{3-\delta}$ > $La_{0.9}Sr_{0.1}Co_{0.5}Cu_{0.5}O_{3-\delta}$ > $La_{0.9}Sr_{0.1}Co_{0.5}Ni_{0.5}O_{3-\delta}$ > $La_{0.9}Sr_{0.1}CoO_3$ > $La_{0.8}Sr_{0.2}CoO_3$ > $La_{0.7}Sr_{0.3}CoO_3$ = $LaCoO_3$ > $LaFeO_3$ > $LaNiO_3$ > $LaZnO_y$. The soot oxidation comparative studies reveal that activity of $La_{0.9}Sr_{0.1}Co_{0.5}Fe_{0.5}O_{3-\delta}$ is far better than Pd-substituted perovskite catalyst.